The Ortho Effect on the Acidic and Alkaline Hydrolysis of Substituted Formanilides

SALIL DILEEP DESAI, LEE E. KIRSCH

Division of Pharmaceutics and Translational Therapeutics, College of Pharmacy, The Dale E. Wurster Center for Pharmaceutical Technology, The University of Iowa, Iowa City, IA 52242

Received 4 February 2015; revised 17 April 2015; accepted 17 April 2015

DOI 10.1002/kin.20925
Published online 9 June 2015 in Wiley Online Library (wileyonlinelibrary.com).

ABSTRACT: The kinetics of formanilides hydrolysis were determined under first-order conditions in hydrochloric acid (0.01–8 M, 20–60°C) and in hydroxide solutions (0.01–3 M, 25 and 40°C). Under acidic conditions, second-order specific acid catalytic constants were used to construct Hammett plots. The *ortho* effect was analyzed using the Fujita–Nishioka method. In alkaline solutions, hydrolysis displayed both first- and second-order dependence in the hydroxide concentration. The specific base catalytic constants were used to construct Hammett plots. *Ortho* effects were evaluated for the first-order dependence on the hydroxide concentration. Formanilide hydrolyzes in acidic solutions by specific acid catalysis, and the kinetic study results were consistent with the $A_{AC}2$ mechanism. *Ortho* substitution led to a decrease in the rates of reaction due to steric inhibition of resonance, retardation due to steric bulk, and through space interactions. The primary hydrolytic pathway in alkaline solutions was consistent with a modified $B_{AC}2$ mechanism. The Hammett plots for hydrolysis of meta- and para-substituted formanilides in 0.10 M sodium hydroxide solutions did not show substituent effects; however, *ortho* substitution led to a decrease in rate constants proportional to the steric bulk of the substituent. © 2015 Wiley Periodicals, Inc. Int J Chem Kinet 47: 471–488, 2015

INTRODUCTION

The hydrolytic instability of formanilides is important to the efficacy of drug molecules [1–5]. A survey of the literature reveals that the effects of *ortho* substitutions on formanilide hydrolysis has not been extensively studied although the effects of *para* and *meta* substitutions are well documented.

In strongly acidic solutions, formanilide has been reported to degrade via the acid-catalyzed acyl cleavage bimolecular ($A_{AC}2$) mechanism [6]. At high concentrations of acid, a linear Hammett relationship was observed for *para* and *meta* substituents. However, at lower acid concentrations a nonlinear Hammett relationship was observed due to a change in the rate-determining step for the reaction. [7,8].

In alkaline solutions, the pH–rate profile for formanilide displayed nonlinear first- and second-order dependence on the hydroxide concentration [9]. Hammett plots showed no difference in reactivity with

Correspondence to: L. E. Kirsch; e-mail: lee-kirsch@uiowa.edu.

change in substituent except for strongly electron-withdrawing compounds such as cyano and nitro groups. Kvalek and Sterba interpreted the alkaline hydrolysis kinetics based on a combination of substrate ionization and the second-order hydroxide-dependent pathway [9]. The Hammett plots were a concave upward curve, suggesting a change in a mechanism or rate-determining step. At lower hydroxide concentrations, kinetics were first order in hydroxide [7,8]. Effects of nucleophilic catalysis, ionic strength, and temperature studies have been studied; however, the results were not mechanistically interpreted [7, 8, 10–12].

More recently, Cheshemdzhieva et al. have investigated the alkaline amide hydrolysis of acetanilides including a series of para-substituted acetanilides wherein the reactivity was correlated to the electrostatic potential of the carbon and nitrogen amide atoms [13,14].

In the present study, the acidic and alkaline hydrolysis kinetics of para- and meta-substituted formanilides are compared to the kinetics of *ortho*-substituted compounds. Substituents were chosen such that they cover the wide range of electronic and steric effects. The substituent constants of the selected substituents are listed in Table I [15,16]. Substrates were synthesized, purified, and characterized and then hydrolyzed under constant pH conditions in acidic and alkaline solutions. Linear-free energy relationships (LFER) and pH-rate profiles were used to evaluate effects of the electronic, steric, and anchimeric factors on acidic and alkaline hydrolysis kinetics and mechanisms.

EXPERIMENTAL

Synthesis

Solvents and chemicals were obtained commercially and used without further purifications. The substituted formanilides were prepared from the unsubstituted anilines by formylation with formic acid using diisopropylether as the solvent (azeotropic synthesis) [17]. The *p*-nitro formanilide was prepared by formylating the *p*-nitro aniline using acetyl formyl anhydride prepared in situ [18]. The volatile formanilides were purified using vacuum distillation, whereas the formanilides with high melting points were purified using recrystalization or extraction. Melting points and purity were determined using a Perkin Elmer DSC7 differential scanning calorimeter [19]. ^{1}H and ^{13}C NMR spectra were recorded at room temperature on a Bruker Avance 300 spectrometer. ^{1}H NMR and ^{13}C NMR spectra were referenced using tetramethylsilane or residual solvent signals as internal standards [20]. Ionization constants (pK_a) were determined for the carboxyl- and hydroxyl-substituted formanilides using potentiometry (*p*-hydroxy (9.58)) and UV spectroscopy (*p*-carboxyl (4.02), *m*-carboxyl (3.86), *o*-carboxyl (3.37), *m*-hydroxyl (9.59), and *o*-hydroxyl(8.98)) [21,22]. The compounds had melting points and NMR spectra in good agreement with literature values [6, 9, 23–39]. The spectra of the compounds not previously synthesized are reported below. The purities of the compounds synthesized were >97%.

N-(3-Methyl phenyl)formamide: δ_H (300 MHz; $CDCl_3$, Me_4Si): 9.6 (br s, ½H), 9.2 (s, ½H), 8.7 (d, ½H), 8.25 (s, ½H), 7.4 (d, 1H, Ar-H), 7.2 (m, 1H, Ar-H), 6.8 (m, 2H, Ar-H), 2.25 (m, 3H, CH_3). δ_C (300 MHz; $CDCl_3$): 163.20, 160.07,139.39, 138.59, 136.98, 136.77, 129.19, 128.57, 125.66, 125.29, 120.76, 119.10, 117.27, 115.39, 21.12, 21.05.

N-(3-Ethylphenyl)formamide: δ_H (300 MHz; $CDCl_3$, Me_4Si): 9.5 (br d, ½H,), 8.75 (d, ½H), 8.60 (br d, ½H,), 8.25 (s, ½H,), 7.40 (m, 1H, Ar-H), 7.2 (m, 1H, Ar-H), 6.9 (m, 2H, Ar-H), 2.60 (m, 2H, CH_2), 1.20 (m, 3H, CH_3). δ_C (300 MHz; $CDCl_3$)163.26, 161.11, 145.93, 145.11, 137.16, 136.88, 129.42, 128.74, 125.59, 124.10, 119.63, 118.16, 117.51, 115.80, 28.64, 28.57, 15.31, 15.29.

N-(3-Isopropylphenyl)formamide: δ_H (300 MHz; $CDCl_3$, Me_4Si): δ 9.45 (br d, ½H), 9.76 (br m, 1H,), 8.35 (s, ½H), 7.50 (m, 1H, Ar-H), 7.25 (m, 1H, Ar-H), 7.0 (m, 2H, Ar-H), 2.8 (m, H, CH), 1.29 (m, 6H, $2CH_3$). δ_C (300 MHz; $CDCl_3$)163.64, 160.18, 151.08, 150.21, 137.47, 137.17, 129.86, 129.17, 123.61, 123.02,118.67, 117.38, 116.44, 34.32, 24.17, 24.13, 24.08.

Kinetic Studies

Hydrolysis reactions were carried out under pseudo–first-order conditions. Reactions in concentrated hydrochloric acid solutions (8.15–0.50 M) and sodium hydroxide solutions (5.0–1.0 M) were followed by using UV spectroscopy. Reactions in dilute hydrochloric acid solutions (0.50–0.010 M) and dilute sodium hydroxide solutions were followed using HPLC.

For studies conducted using HPLC analysis, the following protocol was used. A 10 mM stock solution of the formanilide substrate was prepared in absolute ethanol. A 10-mL of aliquot of dilute hydrochloric acid solution or sodium hydroxide solution was equilibrated to the reaction temperature. Reactions were initiated by adding 0.1 mL of the stock solution of the substrate to the acidic or alkaline solution to give an initial substrate concentration equal to 0.1 mM formanilide and 1% v/v ethanol. Aliquots were withdrawn and quenched with either acetate buffer (1.0 M, pH 4) or tris buffer (1.0 M,

Table I Compilations of the substituent parameters; second order rate constants (40° C) and activation parameters for acidic hydrolysis; and first order rate constants for alkaline hydrolysis (0.1 M sodium hydroxide at 40° C) of substituted formanilides used in this study

								Acidic			Alkaline
Substituent	σ_m	σ_p	σ_m^+	σ_p^+	σ_p^-	E_s[a]	F	$k_H \pm$ SE (M^{-1} h^{-1})	$\Delta H^{\ddagger} \pm$ SE (kJ mol^{-1})	$-\Delta S^{\ddagger} \pm$ SE (J mol^{-1} K^{-1})	k_{obs} ($h^{-1} \times 10^1$)
H	0							7.39 ± 0.08	71.7 ± 2.8	69.3 ± 9.1	4.08
p-CH_3		–0.17		–0.31				5.06 ± 0.11	66.5 ± 0.5	88.7 ± 1.6	3.51
m-CH_3	–0.07		–0.07					6.58 ± 0.18	66.5 ± 1.0	85.8 ± 3.3	3.24
o-CH_3						–1.24	–0.04	2.57 ± 0.04	68.0 ± 0.9	89.7 ± 2.8	0.99
p-Cl		0.23		0.11				7.04 ± 0.07	66.7 ± 1.1	84.6 ± 3.5	3.56
m-Cl	0.37		0.4					9.65 ± 0.02	65.0 ± 0.9	87.4 ± 3.0	3.2
o-Cl						–0.97	0.41	7.24 ± 0.03	65.0 ± 0.8	89.7 ± 2.6	2.05
p-NO_2		0.78		0.79	1.24			27.3 ± 0.7	60.3 ± 0.7	93.5 ± 2.1	1510
m-NO_2	0.71		0.67					11.3 ± 0.2	64.4 ± 0.9	87.9 ± 2.8	4.13
o-NO_2						–1.01[b], –2.52[c]	0.67	24.9 ± 0.2	61.2 ± 0.7	91.8 ± 2.2	2950
p-Br		0.23		0.15				8.32 ± 0.19	67.3 ± 0.6	81.9 ± 2.0	3.39
m-Br	0.39		0.41					10.8 ± 0.1	65.1 ± 0.8	87.1 ± 2.7	2.71
o-Br						–1.16	0.44	2.57 ± 0.04	63.4 ± 1.1	95.5 ± 3.4	3.3
p-C_2H_5		–0.15		–0.3				4.60 ± 0.10	66.6 ± 0.5	87.9 ± 1.7	3.58
m-C_2H_5	–0.07		–0.06					6.21 ± 0.18	63.0 ± 1.2	96.8 ± 3.7	3.01
o-C_2H_5						–1.31	–0.05	2.07 ± 0.01	73.1 ± 2.4	75.4 ± 7.3	0.75
p-isoC$_3$H$_7$		–0.15		–0.28				5.42 ± 0.10	68.0 ± 1.0	83.1 ± 3.2	3.43
m-isoC$_3$H$_7$	–0.07							6.05 ± 0.13	66.4 ± 0.5	86.4 ± 1.6	2.84
o-isoC$_3$H$_7$						–1.71	–0.05	1.39 ± 0.02	71.4 ± 3.1	83.9 ± 9.7	0.675
p-OCH_3		–0.27		–0.79				2.95 ± 0.03	67.7 ± 1.6	88.3 ± 4.9	3.61
m-OCH_3	0.12		0.05					8.59 ± 0.03			3.09
o-OCH_3						–0.55	0.26	5.23 ± 0.21	65.3 ± 0.8	91.1 ± 2.6	2.54
p-COOH		0.45		0.42	0.73			18.2 ± 0.5	61.9 ± 0.3	91.4 ± 1.1	
m-COOH	0.36		0.32					8.21 ± 0.25	63.6 ± 0.3	92.6 ± 1.0	
o-COOH								24.6 ± 0.3	59.9 ± 0.3	95.6 ± 1.0	
p-OH		–0.37		–0.92			0.29	2.67 ± 0.08	68.4 ± 4.3	87.6 ± 13.4	4.13
m-OH	0.12							7.80 ± 0.02	61.0 ± 1.8	101 ± 6	
o-OH								3.81 ± 0.03	64.8 ± 4.3	95.3 ± 13.2	2.8
p-Phenyl		–0.01		–0.18				7.53 ± 0.18	70.4 ± 1.8	73.6 ± 5.6	2.95
o-Phenyl						–1.01[b], –3.82[c]	0.08	3.17 ± 0.02	63.8 ± 1.8	100 ± 6	0.75

[a]Point of reference of E_s values is shifted to H. [b]Minimum perpendicular dimension. [c]Maximum coplanar dimension. Substituent constants were taken from the compilations by Fujita or Exner.

pH 8), and the samples were stored at 4°C until HPLC analysis. The pH value was measured at the start and end of the reaction at the reaction temperature. The degradation reactions were followed to at least three half lives. Concentration time profiles were generated using standards of authentic formanilides and their corresponding anilines in the appropriate concentration range (0.1–0.05 mM). HPLC analyses were performed on a thermo-separations RP-HPLC system consisting of a UV6000LP diode array detector, AS3000 autoinjector, P4000 pump, and an online membrane degasser. Chromatograms were integrated, and data stored using Chromquest® chromatography data system software (Version 4.0). HPLC conditions and mobile phase compositions are provided in Table II.

For studies conducted using UV analysis (Hewlett Packard HP8453 UV–vis diode array spectrophotometer equipped with a Peltier thermostatted cell holder), a 2.5-mL aliquot of hydrochloric acid or sodium hydroxide solution was equilibrated to the reaction temperature in a closed glass cuvette in the thermostatted cell holder of the HP 8453 spectrophotometer. Reactions

Table II Chromatographic conditions used in the analysis of substituted formanilides

Substituent	Flow Rate (mL/min)	Column	Wavelength (λ) (nm)	Retention Times (min)		Mobile Phase
				Substrate	Aniline	
H	0.8	C	235	2.8	3.6	30:70 ACN:10 mM phosphate buffer pH 7
p-Cl	1	C	239	2.6	3.8	38:62 ACN: water
m-Cl	1	C	240	2.6	4.0	38:62 ACN:10 mM phosphate buffer pH 7.2
o-Cl	1	D	236	1.3	2.3	38:62 ACN:10 mM phosphate buffer pH 7.2
p-Br	1	B	242	3.6	4.2	55:45 ACN: water
m-Br	1	D	242	1.8	2.7	35:65 ACN:10 mM phosphate buffer pH 7.2
o-Br	1	C	230	2.7	5.5	38:62 ACN:10 mM phosphate buffer pH 7
p-CH_3	1.2	C	232	2.9	3.7	30:70 ACN:10 mM phosphate buffer pH 7
m-CH_3	1	C	240	3.3	4.5	30:70 ACN:10 mM phosphate buffer pH 7
o-CH_3	1.2	C	228	2.4	4.0	28:62 ACN:23 mM phosphate buffer pH 7
m-C_2H_5	1	D	230	3.9	5.0	30:70 ACN:10 mM phosphate buffer pH 7.2
o-C_2H_5	1	D	230	2.0	3.6	30:70 ACN:10 mM phosphate buffer pH 7.2
p-isoC_3H_7	1	D	231	4.2	5.6	32:68 ACN:10 mM phosphate buffer pH 7.2
m-isoC_3H_7	1	D	231	4.2	5.9	32:68 ACN:10 mM phosphate buffer pH 7.2
o-isoC_3H_7	1	D	231	2.7	5.3	32:68 ACN:10 mM phosphate buffer pH 7.2
p-NO_2	1.2	D	340	6.9	5.6	11:89 ACN:10 mM phosphate buffer pH 7.2
m-NO_2	1	D	236	3.3	4.3	20:80 ACN:10 mM phosphate buffer pH 7.2
o-NO_2	1	D	233	4.0	2.2	25:75 ACN:10 mM phosphate buffer pH 7.2
p-Phenyl	1	D	270	4.1	5.6	35:65 ACN:10 mM phosphate buffer pH 7.2
o-Phenyl	1	D	220	3.2	6.8	35:65 ACN:10 mM phosphate buffer pH 7.2
p-COOH	0.8	A	260	2.8	2.3	10:90 ACN:100 mM phosphate buffer pH 7
m-COOH	0.8	A	238	2.8	2.3	10:90 ACN:100 mM phosphate buffer pH 7
o-COOH	0.8	A	235	4.3	2.7	10:90 ACN:100 mM phosphate buffer pH 7
p-OH	1	A	230	5.7	3.7	05:95 ACN:100 mM phosphate buffer pH 7
m-OH	1	A	210	6.8	4.0	05:95 ACN:100 mM phosphate buffer pH 7
o-OH	1.2	B	230	6.5	3.6	05:95 ACN:10 mM phosphate buffer pH 7

Continued

Table II Continued

Substituent	Flow Rate (mL/min)	Column	Wavelength (λ) (nm)	Retention Times (min) Substrate	Retention Times (min) Aniline	Mobile Phase
p-OCH_3	1	A	235	5.2	4.3	20:80 ACN:100 mM phosphate buffer pH 7
m-OCH_3	0.5	D	235	1.9	2.9	40:60 ACN:100 mM phosphate buffer pH 7
o-OCH_3	0.5	D	235	2.2	2.8	40:60 ACN:100 mM phosphate buffer pH 7

Column: A = Zorbax SB-CN, 5 μ, 4.6 × 150 mm: B = Zorbax SB-C8, 5 μ, 4.6 × 150 mm: C = C12 HydroRP Phenomenex, 4 μ, 4.6 × 75 mm; D = Metasil ODS, 5 μ, 4.6 × 500 mm; and ACN = acetonitrile.

were initiated by adding 25 μL of stock solution (10 mM substrate in ethanol) to the reaction mixture, so that the final concentration of ethyl alcohol was 1% v/v and the final concentration of substrate in solution was 0.1 mM. Spectra were collected as a function of time using the kinetics module in the Chemstation® software. Reactions were followed until there was no significant change in spectra with time. Reactions followed to at least three half lives. The pH value was determined at the beginning and end of the reaction at the reaction temperature. The rate constants determined using UV were reproducible within 5% and also matched those determined from the HPLC studies (±10%).

Identity of the hydrolysis products for substituted formanilides was confirmed by comparing the spectra associated with the final reaction mixture to an authentic sample of the predicted end product at the same concentration (i.e., the corresponding aniline and formic acid). Formic acid does not have appreciable absorbance at these concentrations and cannot be detected; however, aniline has a stronger chromophore and could be detected. The spectrum was collected and compared to the spectrum of the final products using the peak purity compare function in the Chemstation® software. The procedures were all identical for all formanilides except for *o*-hydroxyformanilide, which is insoluble in ethanol, and the stock solution was prepared in dimethyl sulfoxide.

Effects of pH and Temperature on Formanilide Hydrolysis Kinetics

The pH–rate profile for the unsubstituted formanilide at 40°C was determined by using aqueous hydrochloric acid solutions in the concentration range between 8.15 and 0.010 M. Hydrochloric acid solutions in the range of 8.15–1.01 M were prepared by diluting concentrated hydrochloric acid in water. Dilute hydrochloric acid solutions below 1.0 M were prepared by diluting certified hydrochloric acid solutions (1.0 or 0.10 M) in water and adjusting the ionic strength to 1.0 using potassium chloride. The pH–rate profiles for the remaining substituted formanilides were determined in aqueous hydrochloric acid solutions in the range of 1–0.01 M.

The pH–rate profiles for selected formanilides (formanilide, *p*-chloroformanilide, *p*-methylformanilide, *p*-methoxyformanilide, and *m*-nitroformanilide) at 25°C were determined by using aqueous sodium hydroxide solutions in the concentration range between 0.010 and 5.0 M. Sodium hydroxide solutions in the range of 1.0–5.0 M were prepared by diluting 10.0 M certified sodium hydroxide solution in carbonate-free water. Dilute sodium hydroxide solutions (<1 M) were prepared by diluting certified sodium hydroxide acid solutions (1.0 or 0.10 M) in carbonate-free water. Ionic strength was not adjusted for these studies.

The effect of structure on the rate of alkaline hydrolysis of substituted formanilides was evaluated by hydrolyzing them in 0.10 M sodium hydroxide solutions at 40°C. The ionic strengths of these solutions were not adjusted, and reactions were followed using HPLC. The *p*-nitroformanilide and *o*-nitro formanilide degrade very rapidly even at low hydroxide concentrations; hence, the rate of degradation of these compounds was studied using UV spectroscopy.

Studies to determine the effects of temperature on formanilide hydrolysis kinetics were carried out in 1 M hydrochloric acid at 20, 30, 40, 50, and 60°C using UV spectroscopy.

RESULTS

Reaction schemes were determined by mass balance and kinetic analysis for all substrates; the general approach is illustrated using unsubstituted formanilide.

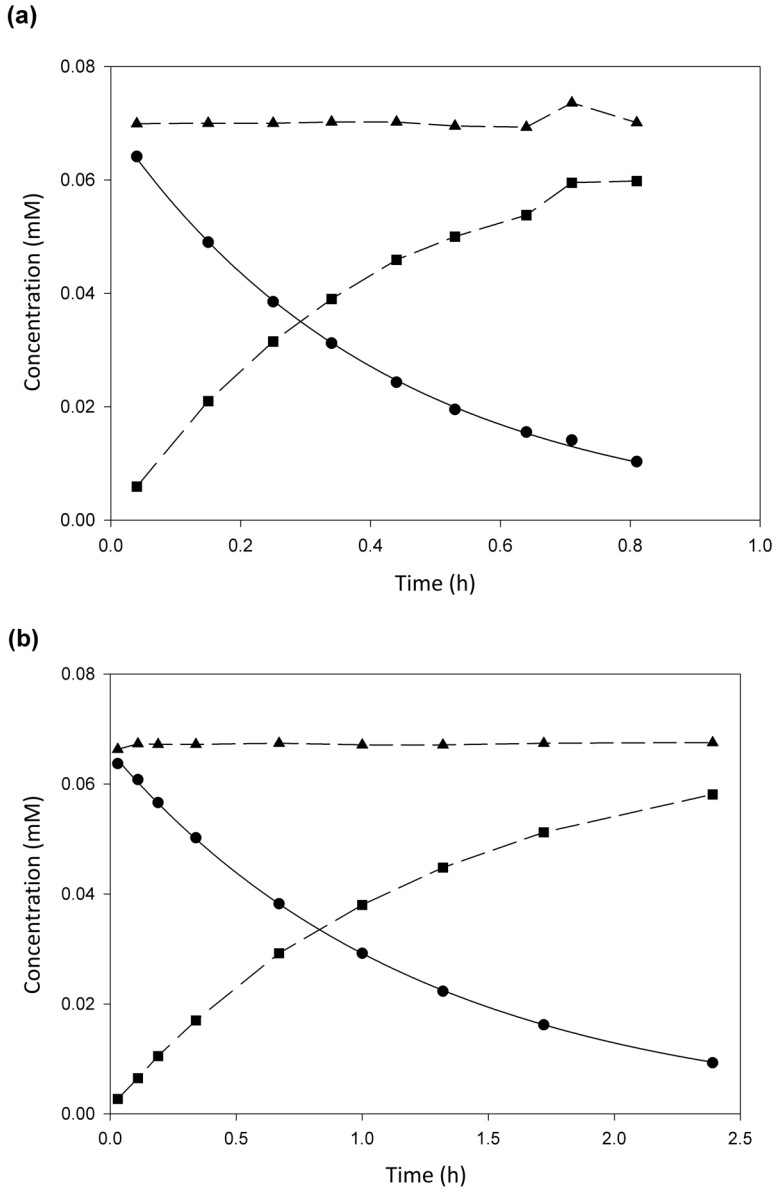

Figure 1 (a) Concentration–time profiles for hydrolysis of formanilide in 0.075 M hydrochloric acid at 1.0 ionic strength and 60°C. (b) Concentration–time profiles for hydrolysis of formanilide in 0.075 M sodium hydroxide solution at 1.0 ionic strength and 60°C. Solid circles (●) represent loss of formanilide, solid squares (■) represent appearance of aniline, and solid triangles (▲) represent mass balance for the reaction. The solid line is a first-order fitting for formanilide loss, and the broken lines are interpolations.

HPLC chromatograms for the acidic and alkaline degradation of formanilide indicated the presence of two compounds identified as the substrate and corresponding aniline. In both cases, the concentration of formanilide decreases as a function of time with a concurrent increase in the concentration of aniline (Fig. 1). The mass balance of the reaction remained constant, which indicated that formanilide quantitatively converted to aniline. Similarly, UV analysis confirmed the presence of a simple mixture composed of substrate and aniline. In acidic solutions the hydrolysis of formanilide produces the anilium ion and formic acid, whereas in alkaline media it forms the aniline and formate ion (Scheme 1).

All of the substituted formanilides hydrolyzed irreversibly to the corresponding substituted aniline, except for *m*-methoxyformanilide (acidic) and *p*- and *o*-hydroxylformanilide. In acidic solutions,

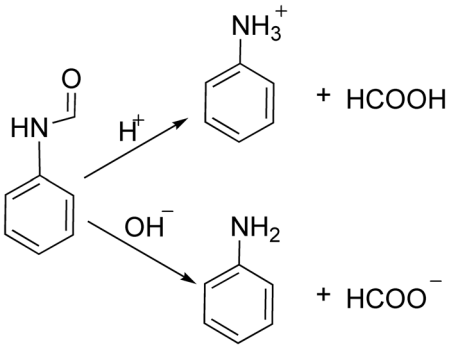

Scheme 1 Reaction scheme for the acidic and alkaline hydrolysis of formanilides.

m-methoxyformanilide degraded to *m*-methoxyaniline; however, mass balance was not maintained. Since *m*-methoxyaniline was found to be stable under identical conditions, parallel loss of *m*-methoxyaniline occurred and the observed rate constant for *m*-methoxyaniline loss (k_{obs}) was the sum of the rate constant (k') for the formation of *m*-methoxyaniline, and the rate constant (k_{unk}) for the parallel loss (Scheme 2). The values for k' and k_{unk} were estimated by nonlinear regression (WinNonlin®).

In alkaline solutions, the concentration–time profiles for *ortho*- and *para*-hydroxyformanilides showed an absence of mass balance due to the rapid degradation of the aniline in alkaline solutions [40]. Thus the estimated k_{obs} value for the loss of the hydroxylformanilides was attributable to the formanilide to aniline conversion.

For all substrates, log-linear substrate concentration –time profiles were used to estimate the observed first-order rate constants (k_{obs}), which were then used to construct pH–rate profiles and to estimate second-order rate constants associated with specific acid or base catalysis. LFER plots were prepared using either first-, second-, or higher order rate constants.

Arrhenius plots were obtained for the temperature dependence of specific acid catalytic constants for the deformylation of substituted formanilides and used to calculate the enthalpies and entropies of activation over the temperature range 20–60°C (Table I).

DISCUSSION

Acid Hydrolysis

The logarithms of the observed rate constants (k_{obs}) were plotted as a function of pH or H_A to construct pH–rate profiles (Fig. 2). For reactions in dilute hydrochloric acid solutions (<1.0 M HCL), the pH values were measured and at high concentrations of hydrochloric acid the H_A scale was used without temperature corrections [41].

A typical bell-shaped pH–rate profile for amide hydrolysis was observed [42]. Formanilide is known to undergo hydrolysis by the $A_{AC}2$ mechanism [6], which predicts a simple pH–rate profile based on the protonation of the carbonyl oxygen at very low pH ($pK_a < -2.5$) followed by solvent attack on the protonated substrate to form the rate-limiting tetrahedral intermediate (Scheme 3). The expected pH rate profile is a downward bend occurring in the pH region of the substrate pK_a and a profile slope of –1 in the pH regions above the pK_a. The observed rate constants decrease as a function of decreasing pH in concentrated acid (below the pK_a) has been attributed to a decrease in water activity [42].

The rate law for the $A_{AC}2$ mechanism can be given by Eq. (1), where $[H^+]$ is the concentration or activity of the hydronium ion; S_{Total} stands for the total substrate concentration; K_a is the ionization constant; k_s is the rate constant for solvolytic hydrolysis of the ionized substrate; and f_{SH} is the fraction of ionized species.

$$\text{Rate} = k_S f_{SH} S_{Total} \tag{1}$$

$$k_{obs} = k_S \frac{[H^+]}{K_a + [H^+]} \tag{2}$$

In dilute hydrochloric acid concentrations (1.0–0.010 M) formanilide is largely unionized ($pK_{BH+} = -2.71$ at 25°C), and, therefore, the hydrolysis rate is first order in the hydronium ion concentration (Eq. (3)) [6]. The second-order rate constant (k_H) as defined in Eqs. (4) and (5) were estimated by linear least-squares fitting of k_{obs} as a function of the

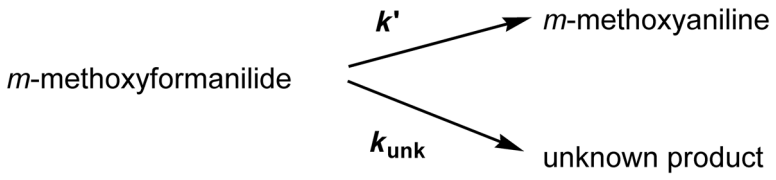

Scheme 2 Reaction scheme for the acid-catalyzed hydrolysis of *m*-methoxyformanilide.

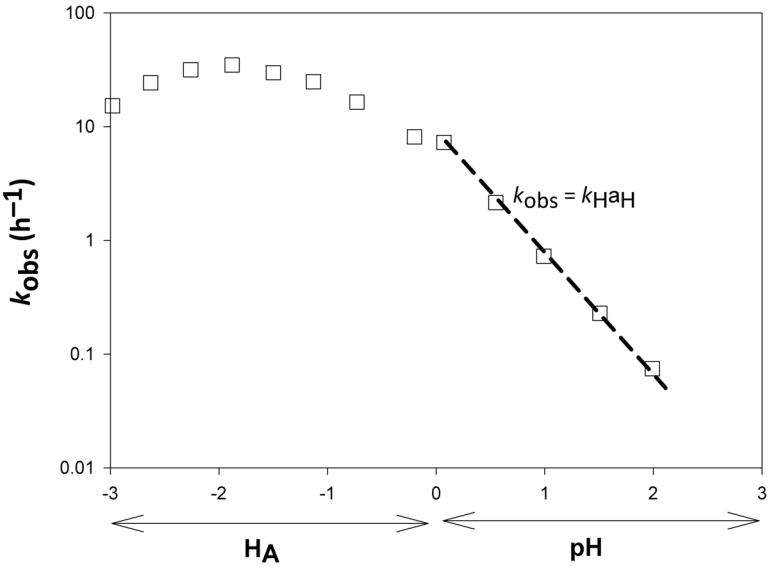

Figure 2 pH–rate profile for formanilide hydrolysis at 40°C in hydrochloric acid solutions. The broken line represents the specific acid-catalyzed region where the slope is –1.

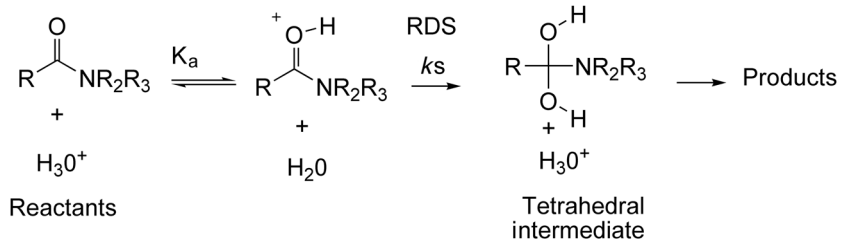

Scheme 3 Acid-catalyzed acyl cleavage bimolecular ($A_{AC}2$) mechanism for hydrolysis of amides.

hydrochloric acid concentration (Table I).

$$k_{\text{obs}} = k_S \frac{[\text{H}^+]}{K_a} \tag{3}$$

$$k_H = \frac{k_S}{K_a} \tag{4}$$

$$k_{\text{obs}} = k_H[\text{H}^+] \tag{5}$$

The pH–rate profiles for the substituted formanilides were similar to formanilide and treated in an analogous manner. For the acidic hydrolysis of m-methoxyformanilide the k′ value was used to estimate kH for that reaction.

The k_H values for *para*- and *meta*-substituted formanilides were used to generate Hammett plots. Under the conditions studied, all of the formanilides were essentially unionized substrates. The Hammett plot is nonlinear and displays downward curvature (Fig. 3A). For *meta*-substituted formanilides, electron-withdrawing substituents (e.g., nitro-, chloro-, bromo-, hydroxyl-, methoxy-, and carboxyl-) displayed an increased rate constant value with increasing electronegativity, whereas electron-donating substituents (e.g., methyl-, isopropyl-, -phenyl, and ethyl-) displayed a decrease with increasing electron-donating capability. Similarly for *para* substituents electronegative substituents (e.g., chloro- and bromo-) exhibited an increase in the k_H, whereas the electron-donating groups (e.g., methyl-, ethyl-, isopropyl-, phenyl-, methoxy-, and hydroxyl-) showed a decrease. These two types of substituents appeared to fall on two separate lines, which intersect at formanilide. Strongly electron-withdrawing substituents capable of resonance interactions (*p*-nitro and *p*-carboxyl) displayed positive deviation from the rest of the compounds.

This type of nonlinear Hammett plot is consistent with a complex mechanism wherein sequential reaction steps possess opposing electronic substituent

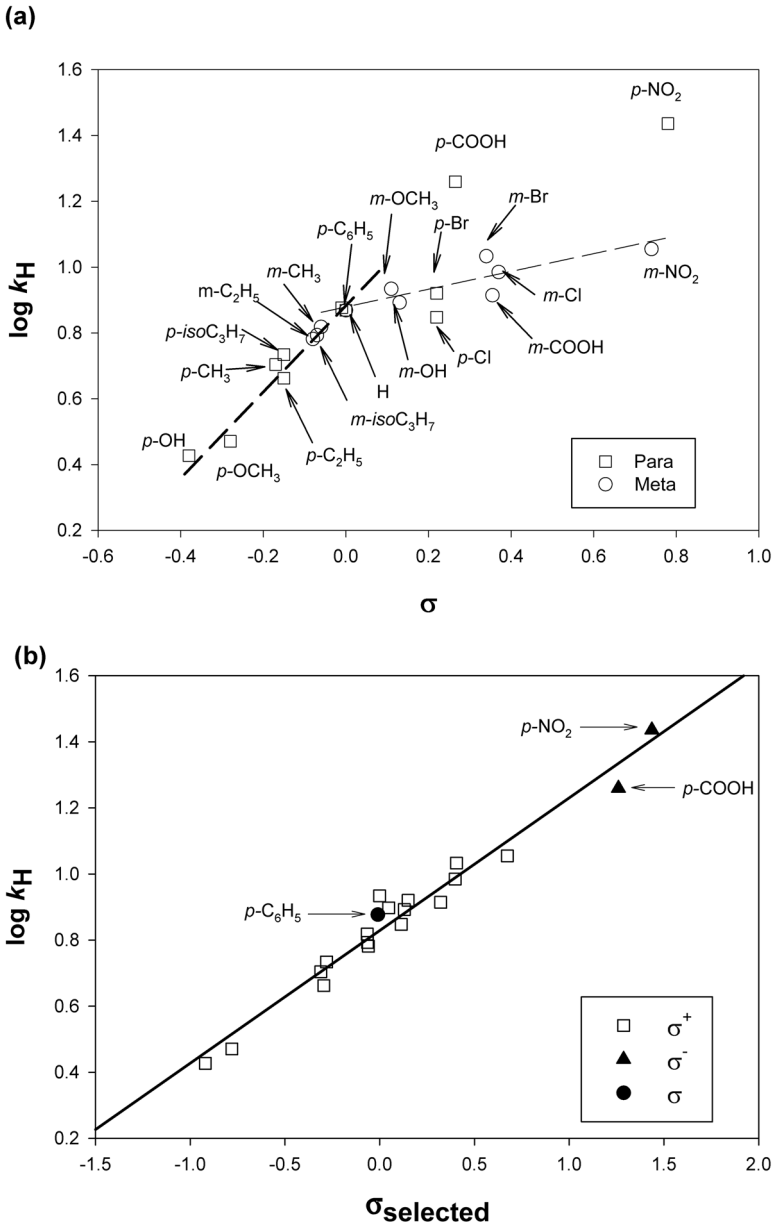

Figure 3 Hammett plots for the acidic hydrolysis of formanilides at 40°C. (a) Hammett sigma values. Broken lines are not fitted to the data (b) selected sigma values. The solid line is a linear fitting to the Hammett equation.

effects that are compensatory, and the second step is rate determining [43]. These results are consistent with the two-step $A_{AC}2$ reaction mechanism in which the second-order rate constant is the ratio of k_s and K_a (Eq. (4)). Thus the overall Hammett reaction constant (ρ) is a function of difference between the reaction constant values for ionization (ρ_{pKa}) and solvent attack steps (ρ_s) (Eq. (6)).

Protonation is enhanced by the electron-donating substituents (ρ_{pKa} = negative), whereas the formation of the tetrahedral intermediate is accelerated by the electron-withdrawing substituents (ρ_s = positive). At the high hydronium concentration, the first step (ionization of the carbonyl oxygen) is not kinetically important since most of the substrate is ionized and thus overall ρ (1.75) is a function of the second step (water attack) [6]. At lower acid concentrations, the first step becomes kinetically important since the ionized fraction of the substrate is significantly reduced and the ρ is a function of both the steps. The ionization

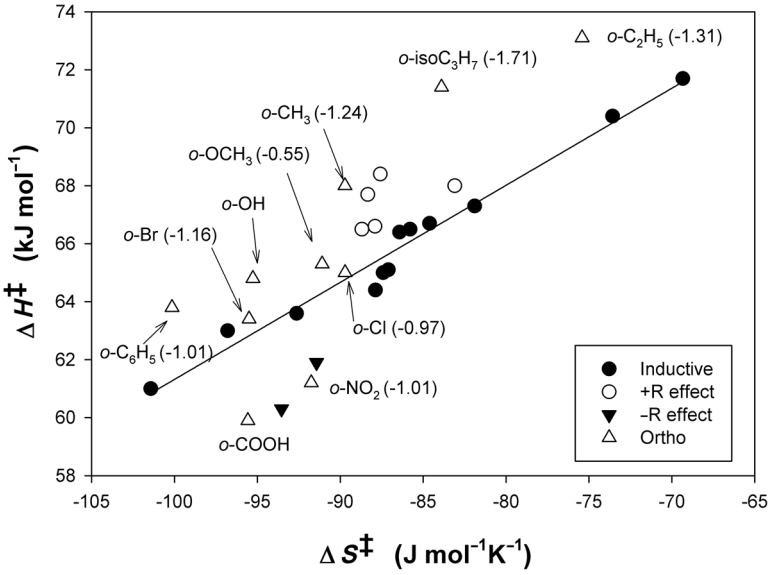

Figure 4 Enthalpy–entropy compensation plot for substituted formanilides. The line is a linear fit to the substituents, which display pure inductive effects. The values in parenthesis are the E_S values.

of formanilides is controlled mainly by inductive effects ($\rho_{\mathrm{pK}a} = -0.48$), but the water attack is influenced strongly by resonance effects [6]. Substituents capable of both inductive and resonance effects affect the both steps, which leads to the curvature in the Hammett plot even though the rate-determining step remains solvolytic attack.

$$\log k_H = (\rho_S + \rho_{pKa})\sigma + c = \rho\sigma + c \qquad (6)$$

An attempt was made to linearize the Hammett plot by selecting the most appropriate substituent constant consistent with the $A_{AC}2$ mechanism and chemical intuition. The Hammett substituent constants (σ) were developed from benzoic acid ionization and represent inductive effects. The substituents with electron-donating capabilities were assigned electrophilic substitution constants (σ^+), whereas those displaying electron-withdrawing capabilities were assigned enhanced sigma constants (σ^-). The σ^+ scale is used in reactions that occur with the development of an electron deficiency, such as aromatic electrophilic substitutions [44]. The σ^+ values are present for most of the *para* substituents and some of the *meta* substituents. If the σ_m^+ value was unavailable, the σ_m value was substituted. The enhanced sigma constants (σ^-) were available for the *p*-nitro and *p*-carboxy groups [45].

This reconstructed Hammett plots displayed linear behavior except for the *p*-phenyl substituent, which deviated from the correlation line using the σ^+ value. Phenyl rings in the para position are capable of resonance interactions only if the phenyl group is planar to the formanilide benzene group. Nonplanar phenyl substituents can interact only through inductive effects. Substituting the appropriate σ values, a Hammett plot with selected sigma values (σ^+, σ, or σ^-) for the para and meta substituents resulted in the LFER relationship displayed in Fig. 3B. This plot was linear with a slope (ρ) of 0.457 ± 0.022 and a correlation coefficient (R^2) value of 0.957. The intercept was 0.843 ± 0.011, which corresponded well to the value for the substituted formanilide (0.869). The value of ρ is positive and indicates that the reaction is accelerated by electron-withdrawing groups. The value of ρ is a composite value and corresponds well to the published ρ value for the acidic hydrolysis of acetanilide (ρ = 0.293, 50% ethanol, 70°C) [46].

Substituent effects can be reflected in activation entropies and enthalpies of the reaction. The enthalpy–entropy plot for *meta*-, *para*-, and *ortho*-substituted formanilides was generated by using activation parameters $\Delta H^{\ddagger}$ and $\Delta S^{\ddagger}$ (Fig. 4). A relationship between the *para*- and *meta*-substituted formanilides was obtained when the substituents were classified into three groups: (1) substituents capable of mainly inductive effects including all the *meta*-substituted formanilides and some *para* substituents (phenyl, chloro, and bromo), (2) substituents that show strong electron-withdrawing capabilities through resonance (–R effects) including the *p*-carboxyl and *p*-nitro substituents, and (3) substituents that show strong electron-donating capabilities

through resonance (+R) including the rest of the *para*-substituted formanilides.

The substituents associated with predominant inductive effects (Group 1) showed a linear correlation ($R^2 = 0.974$), which suggests a common interaction mechanism [47]. This linear relationship is referred to the as the entropy–enthalpy compensation and can be represented by Eq. (7) where β is the compensation temperature and α is a constant. The squared correlation coefficient R^2 value was somewhat less than unity; hence an isokinetic relationship could not be assigned [48]. This observation is consistent with the complex rate law [49]. The compensation temperature (β) is 334 ± 17 K (61.6 ± 17.2°C). At the compensation temperature, the differences in reactivities due to free energy changes become negligible and the substituent effects are muted [45]. The compensation temperature for these substituents is very close to the reaction temperature (40°C) and could account for the small values for the Hammett reaction constant. Groups 2 and 3 substituents show significant deviations from this correlation probably due to their strong electron-donating/accepting capabilities, which affect the interaction mechanisms involved in the hydrolysis.

$$\Delta H^{\ddagger} = \beta \Delta S^{\ddagger} + \alpha \tag{7}$$

In addition to inductive and resonance effects, *ortho* substituents are also capable of steric interactions. Steric interactions include the ability to accelerate or decelerate the reactions due to steric bulk, proximity effects, and anchimeric assistance. A Hammett plot for the *ortho*-substituted formanilides was prepared by assuming that the electronic effects (inductive and resonance) in the *ortho* position were similar to those for corresponding para substituents. The Hammett plot for *ortho*-substituted formanilides has been overlaid on the Hammett plots for the *para* and *meta* formanilides (Fig. 5). The Hammett correlation line based on the *para* and *meta* substituents divides the *ortho*-substituted formanilides into two groups: Those containing oxygen substituents (i.e., *o*-methoxy, *o*-hydroxyl, and *o*-carboxyl) fall above the line, and those bulky substituents without hydrogen-bonding capability fall below the line. An increased rate of hydrolysis for the *o*-hydroxyl group due to anchimeric assistance is possible but fails to explain the rate enhancement observed for the methoxy analog; therefore, electronic field effects may be responsible for the observed rate increases for both analogs. Steric hindrance is the likely cause of the slower hydrolysis rates for *ortho*-substituted methyl, ethyl, nitro, chloro, bromo, isopropyl, and phenyl substrates.

The Taft–Kutter–Hansch steric substituent values (E_s) are noted in Fig. 5A. These values have been derived from the van der Waals dimensions and are indicative of the steric bulk of the substituent. In the *ortho* position, the inductive and resonance effects are higher in the absence of steric bulk effects and the hydrolysis rate of both *o*-carboxyl and *o*-nitro substituent groups should increase. However, the rate constant for the *o*-carboxyl group was nominally higher, and the rate constant for the *o*-nitro group decreased as compared to their *para*-substituted counterparts. This behavior is likely attributable to steric inhibition of resonance for carboxyl and nitro groups.

To investigate the presence of steric inhibition of resonance, the *ortho* substituents were plotted using Hammett sigma (σ_p) values instead of the enhanced sigma values (Fig. 5B). The *o*-hydroxyl and *o*-methoxy substituents fell closer to the correlation line. The methoxy substituent showed a steric substituent effect consistent with its steric bulk. The nitro and phenyl groups have two values associated with them since they are planar groups, and their cross-sectional areas change with the rotation of the group. The reduction in the rate of hydrolysis for the nitro group and the phenyl group are consistent with the value corresponding to the lower E_s value, i.e. the plane of the substituent is perpendicular to the plane of the formanilide benzene ring. Since these substituents are not planar to the ring, the resonance effects of the nitro and phenyl groups were minimal, leaving steric and inductive effects as primary contributors.

The reaction constants of the remaining substituents (chloro, bromo, methyl, ethyl, and *iso*-propyl) all decrease in proportion to their E_s values. The *o*-carboxyformanilide degrades faster than the *p*-carboxyformanilide. This acceleration could be due to the increase in the inductive effect and/or a weak intramolecular catalytic effect.

The Fujita–Nishioka equation (Eq. (8)) was used to describe the steric effects [15]. The equation assumes that the overall rate constant for ortho-substituted compounds is a linear function of three components, i.e. electronic effects, steric effects, and the proximity polar effects. The first term ($\rho\sigma$) corresponds to the electronic effects using various substituent constants (σ_m, σ_p, σ^+, σ^-). The second term (δE_s) corresponds to the steric substituent constants (E_s^{ortho}). The third term (f F) corresponds to the proximity polar effects, which are approximated by the Swain Lupton (F) constant. The reaction constants (ρ, δ, and f) correspond to the electronic, steric, and proximity reaction constants, respectively. The proximity effects and steric terms are only used for *ortho*-substituted compounds. The last term (c) is a constant and corresponds to the logarithm

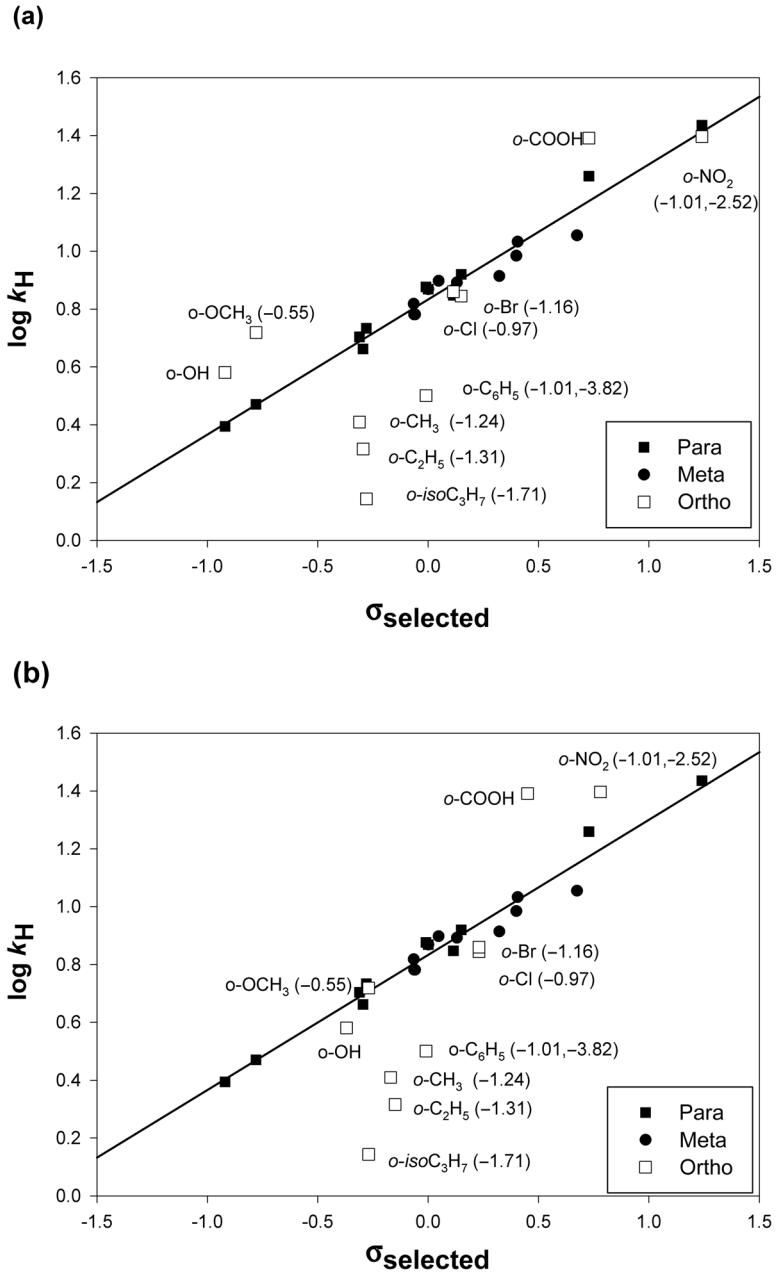

Figure 5 (a) Hammett plots for *para*-, *meta*-, and *ortho*-substituted formanilides using (a) selected sigma values. (b) Hammett plots for *para*-, *meta*-, and *ortho*-substituted formanilides using Hammett sigma values for *ortho* substituents (assuming steric inhibition of resonance). The values in parenthesis are the Taft–Kutter–Hansch values for the steric substituent E_S.

of the unsubstituted compound.

$$\log k_H = \rho\sigma_{o,m,p} + \delta E_S^{\text{ortho}} + fF + c \qquad (8)$$

The substituent constants used for the *para* and *meta* substituents were the same ones used to fit the linear Hammett plot in Fig. 3B. In the *ortho* position, the resonance effects are muted due to the inhibition of resonance hence the Hammett sigma (σ_p) values were used. The E_s values and F values used for the *ortho*-substituted formanilides are given in Table I. The *o*-hydroxyl and *o*-carboxyl substituents were not included in the analysis since E_s and F values are not available for these substituents. Multiple linear regression (JMP®, SAS Institute, Cary, NC) was used to estimate the parameters associated with Eq. (8). The

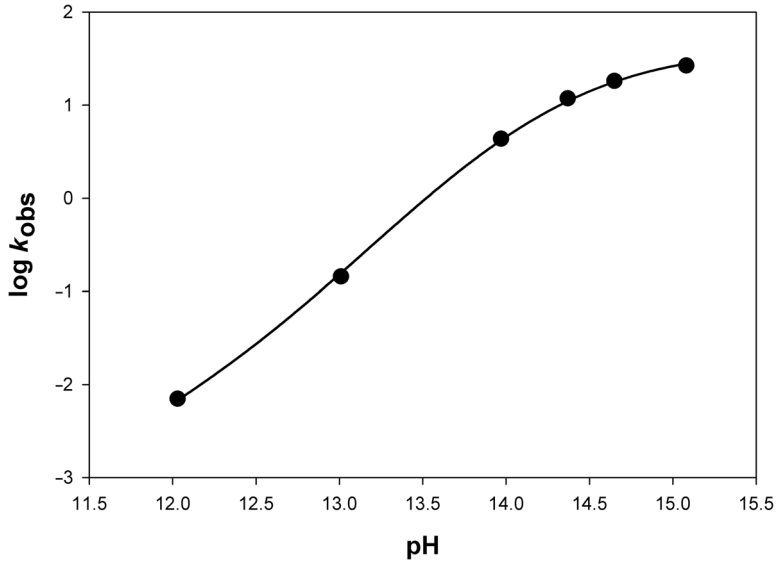

Figure 6 pH–rate profile for alkaline hydrolysis of formanilide using the observed rate constants (k_{obs}) at 25°C. The solid line was simulated using Eq. (9) and estimated from Table II.

adjusted squared correlation constant (R^2 adjusted) value was 0.974. All four terms (ρ, δ, c, and f) were found to be statistically significant by the t test ($p < 0.001$). The F test for the model was significant ($p < 0.001$).

The ρ value, 0.469 ± 0.021, was similar to the value obtained from the Hammett plot for the *para*- and *meta*-substituted formanilides (0.457). The δ parameter had a value of 0.327 ± 0.019. The positive sign indicates steric inhibition, and the magnitude of the steric constant is consistent with minimal crowding at the rate-determining reaction site [15]. The estimated value is consistent with similar reactions, i.e. acidic hydrolysis of phenyl acetates [50].

The f value was 0.697 ± 0.062, which is similar to values seen for other acid-catalyzed hydrolysis reactions [15]. This value was expected to be small as it is the sum of the proximity polar effects of two steps, i.e. ionization of the substrate ($-f$ value), and rate-determining nucleophilic attack ($+f$ value). The intercept value (c) was 0.836 ± 0.011, which corresponds to the value of log k_H for the unsubstituted formanilide (0.869).

The activation enthalpy–entropy plot for the *ortho*-substituted formanilides was also examined (Fig. 4). The *ortho*-substituted formanilides appear to be scattered around the *para*- and *meta*-substituted formanilides. On overlaying the ortho effects against the relationship developed for the *meta* and *para* relationships, the ortho substituents are split into two groups. The *o*-nitro and *o*-carboxyl substituted formanilides lie close to their para counterparts, which is consistent with minimal steric effects and significant inductive effects. The other *ortho* substituents lie above the correlation line associated with inductive effects, indicating the presence of significant *ortho* effects on the hydrolysis reaction [49]. The substituents appear to be distributed randomly without a clear dependence on E_s. Therefore, the *ortho* effect for these substituents appears to be a function of both the steric and proximity effects in agreement with the Fujita–Nishioka analysis.

Alkaline Hydrolysis

The alkaline hydrolysis of formanilide was studied in sodium hydroxide (0.010–3.0 M) solutions at 25°C. At high concentrations of sodium hydroxide, the acidity function (H-, based on the structurally similar thioacetamide) was used. These H-values (obtained from the literature [51,52]) were used to construct the pH–rate profiles (e.g., Fig. 6) wherein the k_{obs} values displayed a dependence on the hydroxide concentration that was higher than first order but less than second order. This behavior has been previously reported for anilides, and the modified base- catalyzed acyl cleavage bimolecular ($B_{AC}2$) mechanism (Scheme 4) involving both a higher order dependence on the hydroxide concentration and reduction in reactive substrate due to ionization has been used for these reactions [53–55]. The unionized substrate can deprotonate to form a conjugate base, which is unreactive, or it can be attacked by the hydroxide ion to form a tetrahedral intermediate that

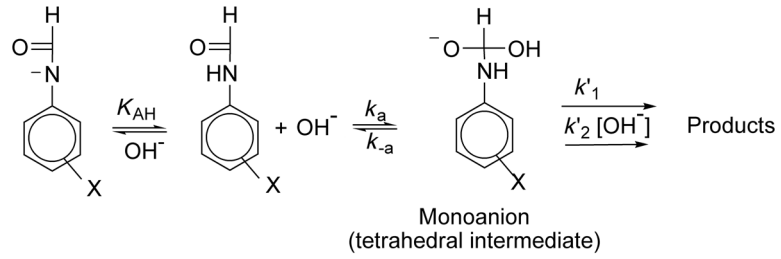

Scheme 4 Modified base catalyzed acyl cleavage bimolecular ($B_{AC}2$) mechanism for hydrolysis of anilides.

subsequently degrades to starting materials or products via water-catalyzed and/or hydroxide-catalyzed pathways.

In Scheme 4, k_a is the rate constant for the addition of the hydroxide ion to the unionized substrate, k_{-a} is the rate constant for the degradation of the intermediate to reactants, k'_1 is the rate constant for the conversion of the intermediate to the products via the water-catalyzed pathway, k'_2 is the rate constant for the conversion of the intermediate to the products via the hydroxide-catalyzed pathway, and K_a is the ionization constant for the formanilide. The rate law is given by Eq. (9), where k_1 is the complex rate constant for the conversion of reactants to products via the water-catalyzed pathway (Eq. (10)); k_2 is the complex rate constant for the conversion of reactant to products via the hydroxide-catalyzed pathway (Eq. (11)); and K_w is the dissociation constant for water.

$$k_{\text{obs}} = \frac{k_1 + k_2[\text{OH}]}{k_a + k_1 + k_2[\text{OH}]} k_a[\text{OH}] \left(\frac{K_w}{[\text{OH}]K_a + K_w} \right) \tag{9}$$

$$k_1 = k'_1 \frac{k_a}{k_{-a}} \tag{10}$$

$$k_2 = k'_2 \frac{k_a}{k_{-a}} \tag{11}$$

The pH–rate profiles for selected substituted formanilides were similar (*p*-chloro, *p*-methyl, *p*-methoxy, and *m*-nitro) to that of formanilide. The pK_a values were taken from the literature (formanilide and *m*-nitroformanilide) or calculated using a Hammett relationship (Eq. (12)) for the ionization constants for formanilides at 20°C using σ^0 (Taft substituent constants for substituents that do not show resonance delocalization interactions) and are given in Table III [9,56].

$$pK_a = -1.52 \times \sigma^0 + 13.8 \tag{12}$$

Nonlinear regression (JMP®, SAS Institute, Cary, NC) was used to estimate k_1, k_2, and k_a values. Rate constant values were weighed using the square of reciprocal of the rate constant [57]. Good agreement between model estimated and observed rate constants as a function of pH (or H-) is depicted in Fig. 6. The estimated rate constants are presented in Table III.

Hammett plots constructed for each pathway were linear with $R^2 > 0.91$. The reaction constant value for k_a (ρ_{ka}) was 1.40 ± 0.09, indicating that the reaction is accelerated by electron-withdrawing groups (Fig. 7). The reaction constant for steps k_1 and k_2 was (ρ_{k1}) -0.23 ± 0.04 and (ρ_{k2}) of 0.63 ± 0.12, respectively, indicating that the reaction process for k_1 was accelerated by electron-donating groups whereas the reaction process for k_2 was accelerated by electron-withdrawing groups.

Table III Rate constants and ionization constants for the base catalyzed hydrolysis of formanilides at 25° C

	pK_a	$k_a \pm$ SE (M^{-1} h^{-1})	$k_1 \pm$ SE (M^{-1} h^{-1})	$k_2 \pm$ SE (M^{-2} h^{-1})
p-Methoxy[c]	14.1[b]	30.7 ± 3.9	0.684 ± 0.117	12.8 ± 1.95
p-Methyl[c]	14.0[b]	40.0 ± 4.7	0.629 ± 0.079	11.2 ± 1.25
H[c]	13.9[a]	51.1 ± 5.0	0.514 ± 0.054	12.6 ± 1.00
p-Chloro[c]	13.4[b]	121 ± 26	0.527 ± 0.113	18.2 ± 2.27
m-Nitro[d]	12.8[a]	760 ± 366	0.389 ± 0.231	50.8 ± 7.70

[a] pK_a values from the literature. [b] pK_a values calculated using the Hammett relationship (Eq. (12)). [c]95% confidence intervals were generated for all parameters. [d]90% confidence intervals were generated for all parameters.

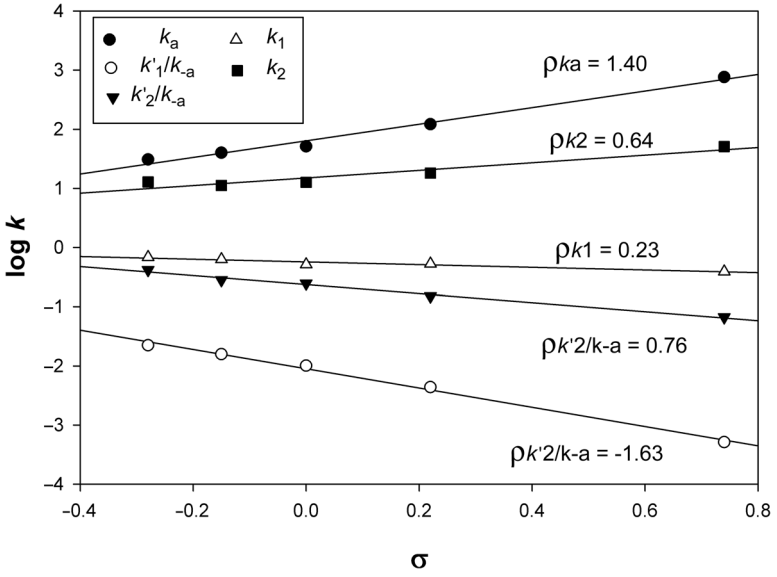

Figure 7 Hammett plots for the rate constants of alkaline hydrolysis of formanilides at 25°C. The lines are linear regression fits of the data to the Hammett equation.

A modified $B_{AC}2$ mechanism is consistent with the Hammett plots. The formation of the tetrahedral intermediate (monoanion) occurs by the addition of hydroxide to the carbonyl carbon. The strong electron-withdrawing groups enhance the susceptibility of the carbonyl carbon to nucleophilic hydroxide attack. The ρ_{ka} value of 1.34 is in agreement with reaction constants for similar reactions such as alkaline hydrolysis of acetanilide (1.0), and 2,2,2-trifluoroacetanlide (1.18) [54,58].

The values for k_1 and k_2 can be explained by a two-step process involving (1) the formation of the intermediate and (2) partitioning of the intermediate to products or reactants. The formation of the intermediate is given by k_a, whereas the partition of the intermediate via k_1 and k_2 processes is given by the partition ratios k_1'/k_{-a} and k_2'/k_{-a}, respectively. The partition ratios were calculated by dividing the complex rate constant k_1 and k_2 with k_a (Eqs. (10) and (11)). In Fig. 7, the Hammett plot for the rate constants (k_a, k_2'/k_{-a} and k_2'/k_{-a}) are shown. The value of the reaction constant ρ_{ka} for the addition step is 1.40, whereas the value of reaction constant for the partition ratio ($\rho_{k1/k-a}$) is -1.63 ± 0.07. The overall reaction constant for the first-order process (ρ_{k1}), –0.23, is the sum of the reaction constants for the two steps.

The magnitude of the substituent effect for the partitioning process predominates the net reaction constant. This value for $\rho_{k1/k-a}$ is comparable to the value of –1.1 obtained in the alkaline hydrolysis of acetanilide where a dipolar ion (Scheme 5) has been hypothesized

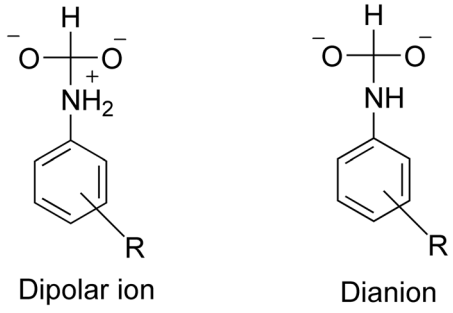

Scheme 5 Hypothetical structures for intermediates in the base-catalyzed hydrolysis of anilides.

to be the rate-limiting intermediate [58]. The dipolar ion is formed by the rate-limiting proton transfer from the hydroxyl group to the amine group by water. The formation of the protonated amine is dependent on the basicity of the nitrogen atom of the anilide. The basicity of the amine is enhanced by electron-donating groups; therefore, the anilines with higher pK_a values will enhance the formation of the dipolar ion. The sign and magnitude of the reaction constant for the amine protonation can be approximated by the reaction constant for the ionization of anilines ($\rho = -2.77$) [46]. The significant negative value for $\rho_{k1/k-a}$ is consistent with this process.

The reaction constant for the pathway involving second-order dependence on hydroxide (described by the rate constant k_2) was estimated to be $+0.63$, and

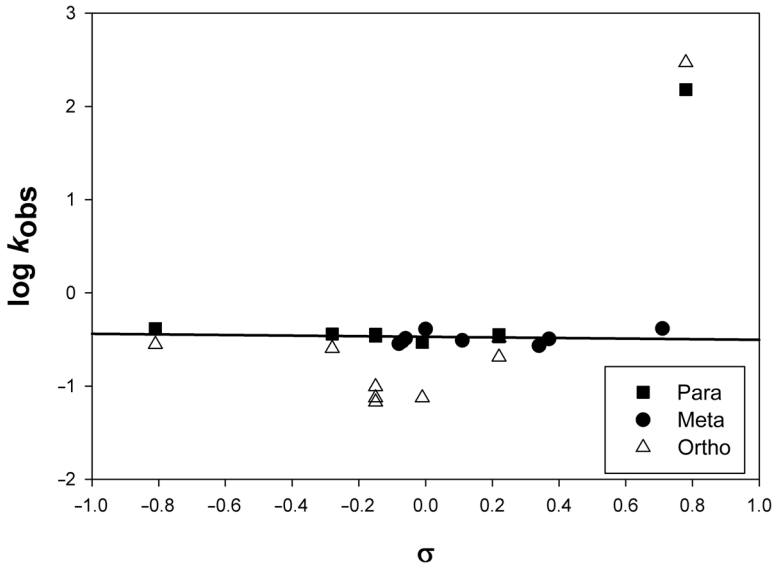

Figure 8 Hammett plots for the hydrolysis of substituted formanilides in 0.10 M sodium hydroxide solutions at 40°C.

the value of the reaction constant for the partition ratio ($\rho_{k2/k-a}$) was –0.76 ± 0.05. This value is significantly smaller than the reaction constant for the addition process and hence the substituent effect for the formation of the intermediate predominates in the net reaction constant ($\rho_{k2} = 0.63$). A likely mechanism for the second-order hydroxide pathway involves formation of a dianion intermediate (Scheme 5) and breakdown to products via rate-determining formation of a dipolar ionic intermediate [54,59]. The formation of the dipolar ion is likely the rate limiting. The rate constant for the second-order reaction (k_2') contains the rate constant for the formation of the dianion and the rate-determining formation of the dipolar ion. The kinetic process for the formation of the dianion is very similar to the kinetic process for the formation of the monoanion, and hence the reaction constant for the formation of the dianion is also expected to be positive. The value of ρ_{k2} is a sum of the positive reaction constant for the dianion formation and negative reaction constant for the formation of the dipolar ion (amine basicity); and hence $\rho_{k2/k-a}$ is only slightly negative.

Owing to the complexity of the kinetic scheme, the effects of *ortho* substitution on each elementary step in a pathway could not be determined. Hence substituent effects were evaluated using the observed first-order rate constant (k_{obs}) estimated from a series of studies conducted under identical experimental conditions (0.10 M sodium hydroxide and 40.0°C). Since the hydroxyl-substituted substrates were primarily deprotonated under the experimental conditions (pKa = 9.6), the phenoxide-substitutent constant (–0.81) was used for *p*-hydroxyformanilide in the Hammett plot (Fig. 8).

Nearly all of the observed first-order rate constants values for the *para*- and *meta*-substituted substrates were within the range of 0.2–0.7 h^{-1}, and therefore appeared to be independent of the Hammett sigma values. These results agree with studies on the alkaline hydrolysis of anilides [58,60]. The estimated k_{obs} value for the *p*-nitro substrate was about 350-fold greater than the other *para*- and *ortho*-substituted substrates, which suggests a different mechanism of alkaline hydrolysis [60–63].

Results from the alkaline hydrolysis of *ortho*-substituted substrates were compared to their *para*-substituted counterparts (Fig. 8). With the exception of the *o*-nitroformaniline, the *ortho* compounds typically degraded more slowly than *para* or *meta* substrates. The degree of stabilization varied from <10% to >80% for the bromine- and *iso*propyl-substituted compounds, respectively. In general, stabilization could be attributed to steric effects using the Taft–Kutter–Hansch treatment (Eq. (13), Fig. 9) wherein a linear correlation was observed between the logarithm of k_{obs} and the Taft–Kutter–Hansch steric substituent value (E_s) with a δ_{app} of 0.505 ± 0.094 and a correlation coefficient (R^2) of 0.8787. The positive sign for the value indicates that the steric bulk inhibits the reaction, whereas the value indicates that the steric bulk inhibition of reaction is significant. Thus the first-order process is inhibited strongly by steric bulk. The rate-limiting states for both the first- and second-order pathways for alkaline hydrolysis of formanilides are

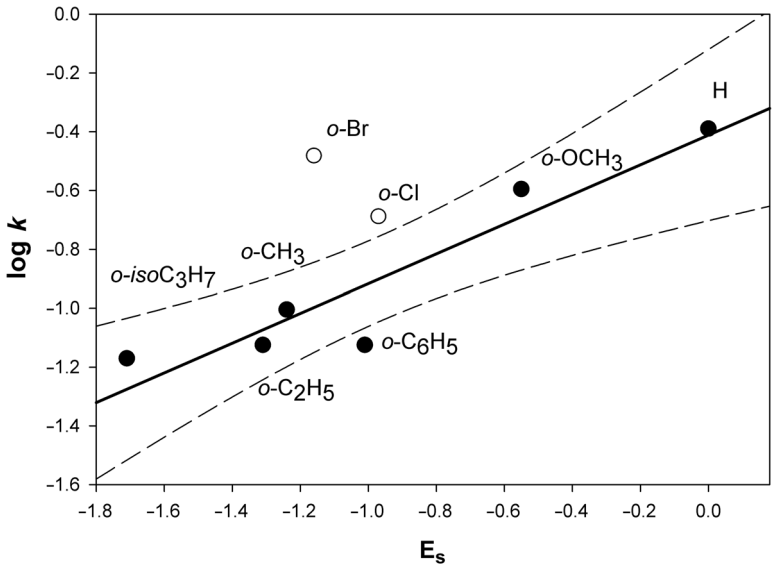

Figure 9 Plot of the logarithm observed rate constants for *ortho*-substituted formanilides versus the steric substituent constant (E_s) determined in 0.10 M sodium hydroxide at 40°C. The solid line indicates the linear correlation line to Eq (13), whereas the broken lines indicate 95% confidence intervals. The substituents included in the regression analysis are denoted by solid circles (●) and those not included are denoted by open circles (○).

similar, and, therefore, it is possible that the steric bulk inhibition effect will be similar for both the pathways.

$$\log k_{obs} = \delta_{app} E_s + c \tag{13}$$

The relative instability of the *o*-nitro substituent is similar to *p*-nitroformanilide, which may degrade by a different pathway then the other substituted formanilides. The *o*-bromo and *o*-chloro substituents are strongly electron withdrawing, and thus the second-order hydroxide pathway may play a predominant role in their alkaline hydrolysis. These substrates were not considered in evaluating steric effects using Eq. (13).

CONCLUSION

The acidic hydrolyses of formanilides occurs by the $A_{AC}2$ mechanism and showed nonlinear Hammett plots. The nonlinear Hammett plots were explained using the two-step $A_{AC}2$ mechanism. *Ortho* substitution led to inhibition of resonance between the substituent and reaction site by disrupting the planarity of the amide group with the phenyl ring. The analysis of the *ortho* effect using Fujita–Nishioka analysis showed the presence of steric bulk and through space effects. No evidence of anchimeric assistance was observed for *ortho*-substituted substrates.

The alkaline hydrolyses showed first- and second-order dependence on hydroxide, which be explained adequately by the modified $B_{AC}2$ mechanism. The Hammett plots for each step were found to be consistent with the $B_{AC}2$ mechanism. *Ortho* effects in alkaline were found to be primarily dependent on steric bulk.

BIBLIOGRAPHY

1. Yoshioka, S.; Stella, V. J. Stability of Drugs and Dosage Forms; Kluwer: New York, 2000; pp. 3–137.
2. Wang, W. Int J Pharm 1999, 185(2), 129–188.
3. Ma, M.; Sun G. Dyes Pigm 2004, 63(1), 39–49.
4. Brown, R. S. In The Amide Linkage: Selected Structural Aspects in Chemistry Biochemistry and Material Science; Greenberg, A.; Breneman, C. M.; Liebman, J. F., Eds.; Wiley: New York, 2000; pp. 85–114.
5. Challis, B. C.; Challis J. In The Chemistry of Amides; Zabicky, J., Ed.; Interscience: New York, 1970; pp. 731–858.
6. Kavalek, J.; Sterba V. Collect Czech Chem Commun 1975, 40(6), 1924–1231.
7. Bergstrand, B. Acta Pharm Suec 1983, 20(2), 81–98.
8. Bergstrand, B. Acta Pharm Suec 1984, 21(1), 43–54.
9. Kavalek, J.; Sterba V. Collect Czech Chem Commun 1975, 40(4), 1176–1182.
10. Bergstrand, B. Acta Pharm Suec 1984, 21(1), 55–66.
11. Bergstrand, B. Acta Pharm Suec 1985, 22(1), 1–16.
12. Bergstrand, B.; Sundelof L. O. Acta Pharm Suec 1981, 18(5), 283–298.

13. Cheshmedzhieva, D.; Ilieva, S.; Hajieva, B.; Galabov, B. J Phys Org Chem 2009, 22(6),619–631.
14. Cheshmedzhieva, D.; Ilieva, S.; Hajieva, B.; Trayanova, T.; Galabov, B. Mol Phys 2009, 107, 1187–1192.
15. Fujita, T.; Nishioka, T. In Progress in Physical Organic Chemistry; Taft, R. W., Ed.; Wiley: New York, 1976; pp. 49–89.
16. Exner, O. In Correlation Analysis in Chemistry: Recent Advances; Chapman, N. B.; Shorter, J., Eds. Plenum Press: New York, 1978; pp. 439–540.
17. Werner, W. J Chem Res, Synop 1981(4), 120–120.
18. Huffman, C. W. J Org Chem 1958, 23(5),727–729.
19. Plato, C.; Glasgow, Jr A. R. Analyt Chem 1969, 41(2), 330–336.
20. Gottlieb, H. E.; Kotlyar, V.; Nudelman, V. J Org Chem 1997, 62(21), 7512–7515.
21. Gran, G. Analyst 1952, 77, 661–671.
22. Albert, A.; Serjeant E. P. The Determination of Ionization Constants: A Laboratory Manual; Chapman and Hall: New York, 1984; pp. 70–73.
23. Hosseini-Sarvari, M.; Sharghi H. J Org Chem 2006, 71(17), 6652–6654.
24. Yale, H. L. J Org Chem 1971, 36(21), 3238–3240.
25. Hill, D. R.; Hsiao, C. N.; Kurukulasuriya, R.; Wittenberger, S. J. Org Lett 2002, 4(1), 111–113.
26. Di Nunno, L.; Scilimati, A. Tetrahedron 1986, 42(14), 3913–3920.
27. Pettit, G. R.; Kalnins, M. Liu, T.; Thomas, E.; Parent, K. J Org Chem 1961, 26, 2563–2566.
28. Berrier, C.; Jacquesy, J. C.; Jouannetaud, M. P.; Morellet, G. Bull Soc Chim Fr 1987(1), 158–164.
29. Farley, T. M.; Strong, F. M.; Bydalek, T. J. J Am Chem Soc 1965, 87(15), 3501–3504.
30. Pettit, G. R.; Thomas, E. G. J Org Chem 1959, 24, 895–896.
31. Exner, O.; Lakomy, J. Collect Czech Chem Comm 1970, 35(5), 1371–1386.
32. Buss, C. E.; Mann, K. R. J Am Chem Soc 2002, 124(6), 1031–1039.
33. Wiberg, K. B.; Shryne, T. M.; Kintner, R. R. J Am Chem Soc 1957, 79, 3160–3164.
34. Lesiak, T. Chem Stosowana, Ser A, 1963, 7(4), 593–601.
35. Gim, H. J.; Kang, B. M.; Jeon, R. Arch Pharm Res 2007, 30(9), 1055–1061.
36. Arient, J.; Dovorak, J. Chem Listy Vedu Prum 1956, 50, 1636–1638.
37. Zimmermann, J. Ber Dtsch Chem Ges 1880, 13(2), 1963–1969.
38. Kisfaludy, L.; Otvos, L., Jr. Synthesis 1987(5), 510.
39. Kamer, P. C. J.; Nolte, R. J. M.; Drenth, W. J Am Chem Soc 1988, 110(20), 6818–6825.
40. Koshy, K. T.; Lach, J. L. J Pharm Sci 1961, 50(2), 113–118.
41. Yates, K.; Riordan, J. C. Can J Chem 1965, 43(8), 2328–2335.
42. Bruice, T. C.; Benkovic, S. Bioorganic Mechansims; W. A. Benjamin: New York, 1966; pp. 1–211.
43. Jencks, W. P. Catalysis in Chemistry and Enzymology; Dover: New York, 1987; pp. 480–483.
44. Brown, H. C.; Okamoto, Y. J Am Chem Soc 1958, 80, 4979–4987.
45. Connors, K. A. Chemical Kinetics: The Study of Reaction Rates in Solution; VCH: New York, 1990; pp. 311–384.
46. Jaffe, H. H. Chem Rev 1953, 53, 191–261.
47. Leffler, J. E.; Grunwald, E. Rates and Equilibria of Organic Reactions. Dover: New York, 1989; pp. 128–170.
48. Liu, L.; Guo, Q.-X. Chem Rev 2001, 101, 673–695.
49. Leffler, J. E.; Grunwald, E. Rates and Equilibria of Organic Reactions; Dover: New York, 1989; pp. 315–402.
50. Nishioka, T.; et al. Fujira, T.; Kitamura, K.; Nakajima, M. J Org Chem. 1975, 40(17), 2520–2525.
51. Edward, J. T.; Wang, I. C. Can J Chem 1962, 40, 399–408.
52. Bowden, K.; Bromley, K. J Chem Soc, Perkin Trans 2: Phys Org Chem 1990(12), 2103–2109.
53. Biechler, S. S.; Taft, R. W. J Am Chem Soc 1957, 79(18), 4927–4935.
54. Kershner, L. D.; Schowen, R. L. J Am Chem Soc 1971, 93(8), 2014–2024.
55. Eriksson, S. O. Acta Pharm Suec 1969, 6(2), 121–138.
56. Yukawa, Y.; Tsuno, Y.; Sawada, M. Bull Chem Soc Jpn 1972, 45(4), 1198–1205.
57. Motulsky, H.; Christopoulos, A. Fitting Models to Biological Data Using Linear and NonLinear Regression. A Practical Guide to Curve Fitting; GraphPad Software: San Diego CA, 2003; pp. 84–89.
58. Bender, M. L.; Thomas, R. J. J Am Chem Soc 1961, 83(20), 4183–4189.
59. Schowen, R. L.; Jayaraman, H. Kershner, L.; Zuorick, G. W. J Am Chem Soc 1966, 88(17), 4008–4012.
60. DeWolfe, R. H.; Newcomb, R. C. J Org Chem 1971, 36(25), 3870–3878.
61. Sorci, J. J.; Macalady, D. L. J Agric Food Chem 1993, 41(10), 1760–1766.
62. Pollack, R. M.; Bender, M. L. J Am Chem Soc 1970, 92(24), 7190–7194.
63. Broxton, T. J.; Deady, L. W. J Org Chem 1975, 40(20), 2906–2910.